

---

1 **Evaporation and sublimation measurement and modelling of an alpine saline lake influenced by**  
2 **freeze–thaw on the Qinghai–Tibet Plateau**

3 Fangzhong Shi<sup>1,2,3</sup>, Xiaoyan Li<sup>1,2,4,5</sup>, Shaojie Zhao<sup>1,2</sup>, Yujun Ma<sup>6</sup>, Junqi Wei<sup>1,2</sup>, Qiwen Liao<sup>1,2</sup>, Deliang  
4 Chen<sup>7</sup>

5 <sup>1</sup>State Key Laboratory of Earth Surface Processes and Resource Ecology, Faculty of Geographical  
6 Science, Beijing Normal University, Beijing 100875, China;

7 <sup>2</sup>School of Natural Resources, Faculty of Geographical Science, Beijing Normal University, Beijing  
8 100875, China

9 <sup>3</sup>Research and Development Center for Watershed Environmental Eco–Engineering, Beijing Normal  
10 University at Zhuhai, Zhuhai, 519085, China;

11 <sup>4</sup>Key Laboratory of Tibetan Plateau Land Surface Processes and Ecological Conservation, Ministry of  
12 Education, Qinghai Normal University, Xining, China

13 <sup>5</sup>Academy of Plateau Science and Sustainability, Qinghai Normal University, Xining, China

14 <sup>6</sup>School of Geography and Planning, Sun Yat–sen University, Guangzhou, China

15 <sup>7</sup>Regional Climate Group, Department of Earth Sciences, University of Gothenburg, Gothenburg,  
16 Sweden.

17 \* To whom the correspondence should be addressed: Xiao–Yan Li, State Key Laboratory of Earth  
18 Surface Processes and Resource Ecology, Beijing Normal University, Beijing, China. Emails:  
19 xyli@bnu.edu.cn.

20

---

21

22 **Key Points**

- 23 ● Night evaporation of Qinghai Lake accounts for more than 40% of the daily evaporation during  
24 both the ice-free and ice-covered periods.
- 25 ● Lake ice sublimation reaches  $175.22 \pm 45.98$  mm, accounting for 23% of the annual evaporation.
- 26 ● Wind speed weakening may have resulted in an 7.56% decrease in lake evaporation during the  
27 ice-covered period from 2003 to 2017.

---

28 **Abstract**

29 Saline lakes on the Qinghai–Tibet Plateau (QTP) affect the regional climate and water cycle through  
30 water loss (E, evaporation under ice–free and sublimation under ice–covered conditions). Due to the  
31 observation difficulty over lakes, E and its underlying driving forces are seldom studied targeting saline  
32 lakes on the QTP, particularly during the ice–covered periods (ICP). In this study, The E of Qinghai Lake  
33 (QHL) and its influencing factors during the ice–free periods (IFP) and ICP were first quantified based  
34 on six years of observations. Subsequently, three models were calibrated and compared in simulating E  
35 during the IFP and ICP from 2003 to 2017. The annual E sum of QHL is  $768.58 \pm 28.73$  mm, and the E  
36 sum during the ICP reaches  $175.22 \pm 45.98$  mm, accounting for 23% of the annual E sum. E is mainly  
37 controlled by the wind speed, vapor pressure difference, and air pressure during the IFP, but is driven by  
38 the net radiation, the difference between the air and lake surface temperatures, wind speed, and ice  
39 coverage during the ICP. The mass transfer model simulates lake E well during the IFP, and the model  
40 based on energy achieves a good simulation during the ICP. Moreover, wind speed weakening resulted  
41 in an 7.56% decrease in E during the ICP of 2003~2017. Our results highlight the importance of E in ICP,  
42 provide new insights into saline lake E in alpine regions, and can be used as a reference to further improve  
43 hydrological models of alpine lakes.

44 **Keywords:**

45 Lake evaporation and sublimation, saline lakes, flux observation, ice–covered periods, Qinghai Lake,  
46 Qinghai–Tibet Plateau

---

## 47 1. Introduction

48 Saline lakes account for 23% of the total area and 44% of the total water volume of Earth's lakes  
49 (Wurtsbaugh et al., 2017). They are critical in shaping the regional climate and maintaining ecological  
50 security and sustainable development in arid regions (Messenger et al., 2016; Wurtsbaugh et al., 2017;  
51 Woolway et al., 2020; Wu et al., 2021; Wu et al., 2022). Under the influences of climate change and  
52 human activities, saline lakes worldwide have changed rapidly in terms of their area, level, temperature,  
53 ice phenology, energy, and water exchange, which has become an issue of concern (Gross, 2017;  
54 Wurtsbaugh et al., 2017; Woolway et al., 2020). Evaporation under ice-free periods (IFP) and  
55 sublimation under ice-covered periods (ICP) are important mechanisms of the transfer of energy and  
56 water between lakes and the atmosphere, and are among the major factors influencing changes in lake  
57 water volume (Ma et al., 2016; Zhu et al., 2016; Woolway et al., 2018; Guo et al., 2019; Woolway et al.,  
58 2020).

59 In contrast to freshwater lakes, E (evaporation under IFP and sublimation under ICP) of saline lakes  
60 involves a more complex process and is affected not only by climate conditions, lake depth, temperature,  
61 stratification, thermal stability, and hydrodynamics, but also by salinity (Salhotra et al., 1985; Hamdani  
62 et al., 2018; Obiany, 2019; Woolway et al., 2020). For example, dissolved salt ions can reduce the free  
63 energy of water molecules (i.e., reduce water activity) and result in a reduced saturated vapor pressure  
64 above saline lakes at a given water temperature (Salhotra et al., 1987; Mor et al., 2018). Previous studies  
65 have investigated the relationship between the E and salinity of saline lakes, and discrepancies in the  
66 controlling factors between different time scales (Salhotra et al., 1987; Lensky et al., 2018; Hamdani et  
67 al., 2018; Mor et al., 2018). These studies have mainly focused on saline lakes in arid and temperate  
68 zones, and the interaction and mutual feedback between the water body of saline lakes and the  
69 atmosphere remain unclear. There are few studies on the E of alpine saline lakes that exhibit complex  
70 hydrology and limnology.

71 Saline lakes account for over 70% of the total lake area on the Qinghai-Tibet Plateau (QTP) (Liu et al.,  
72 2021), and thus profoundly affect the regional climate and water cycle through the E (Yang et al., 2021).  
73 However, continuous year-round direct measurements of saline lake E are scarce, which hinders the  
74 exploration of lake E at different time scales. Observations of E from saline lakes have been obtained for

---

75 Qinghai Lake (QHL) (Li et al., 2016), Namco (Wang et al., 2015; Ma et al., 2016), Selinco (Guo et al.,  
76 2016), and Erhai (Liu et al., 2015) via the eddy-covariance (EC) technique or pan E on the QTP, but  
77 these observations are mainly during the IFP (approximately mid-May to mid-October). Thus, there are  
78 considerably fewer E observations during the ICP and full-year period of lakes, mostly because of the  
79 harsh environment and limited accessibility to the QTP (Zhu et al., 2016). However, most lakes on the  
80 QTP exhibit a long and stable ICP lasting more than 100 days due to the low annual air temperature ( $T_a$ )  
81 (Cai et al., 2019), which suggests that E observations are currently lacking for nearly a quarter of the year  
82 (from the IFP to the ICP). Although studies have commented on the importance of E during the ICP (Li  
83 et al., 2016; Wang et al., 2020), and clarified that freezing/breakup processes could result in sudden  
84 changes in lake surface properties (such as albedo and roughness) and affect the water and energy  
85 exchange between the lake and atmosphere (Cai et al., 2019; Yang et al., 2021). the dynamic processes  
86 of energy interchange and E of saline lakes during the ICP and its responses to climatic variability on the  
87 QTP still constitute a knowledge gap in lake hydrology research. Thus, there is an urgent need to better  
88 quantify lake E during the ICP on the QTP.

89 Many models have been employed to calculate lake E, mainly including the Dalton formula series based  
90 on mass transfer and aerodynamics, energy and water balance formula series, Penman formula series  
91 considering both aerodynamics and energy balance, and empirical formulas based on statistical analysis  
92 (Dalton, 1802; Bowen, 1926; Penman, 1948; Harbeck et al., 1958; Finch and Calver, 2008; Hamdani et  
93 al., 2018; Wang et al., 2019a). However, the reported values exhibit large discrepancies in their seasonal  
94 variations and annual amounts between those models (Zhu et al., 2016; Ma et al., 2016; Guo et al., 2019;  
95 Wang et al., 2019a; Wang et al., 2020), and almost all models were calibrated and verified against E  
96 observations during the IFP, while E during the ICP was either not calculated or unverified (Wang et al.,  
97 2020), as a result of the deficiency in observed E during the ICP (Zhu et al., 2016; Guo et al., 2019). In  
98 addition, compared with small lakes, large and deep lakes exhibit higher E levels and delayed seasonal  
99 E peaks because more energy is absorbed and stored in large and deep lakes during the IFP and released  
100 during the ICP (Wang et al., 2019a). Thus, the effect of changes in ice phenology on lake E is particularly  
101 important, which calls for different models for E simulation during the IFP and ICP.

102 Furthermore, with increasing overall surface air warming and moistening, solar dimming, and wind

---

103 stilling since the beginning of the 1980s (Yang et al., 2014), lakes on the QTP have experienced a  
104 significant temperature increase (at a rate of  $0.037\text{ }^{\circ}\text{C yr}^{-1}$  from 2001 to 2015) (Wan et al., 2018) and ice  
105 phenology shortening (at a rate of  $-0.73\text{ d yr}^{-1}$  from 2001 to 2017) (Cai et al., 2019). Changes in  $T_a$ ,  
106 water surface temperature ( $T_s$ ), wind speed (WS), and ice phenology could impose different effects on  
107 energy interchange and molecular diffusion due to differences in the state phase and reflectance of water  
108 between the ICP and IFP, thus altering lake E (Wang et al., 2018). Although many studies have reported  
109 a decrease in lake E on the QTP by model simulations (Ma et al., 2016; Zhu et al., 2016; Li et al., 2017;  
110 Guo et al., 2019), owing to E neglect during the ICP, the potential mechanisms of lake E and its different  
111 responses to climate variability during the ICP and IFP remain unclear.

112 In this study, based on six continuous years of direct measurements of lake E and energy exchange flux  
113 data obtained with the EC technique pertaining to QHL, the largest saline lake on the QTP, between 2014  
114 and 2019, we quantified the characteristics of energy interchange and E on diurnal, seasonal (IFP, ICP  
115 and cycle year: AN) and yearly time scales and identified the potential factors influencing E during the  
116 IFP and ICP. In addition, combined with reanalysis climate datasets, a mass transfer model (MT model),  
117 an atmospheric dynamics model (AD model), and a model based on energy, temperature and WS (JH  
118 model) were calibrated and verified, with the optimal model chosen for the simulation of lake E and its  
119 response to climatic variability during the IFP and ICP from 2003 to 2017. The results highlight the  
120 importance and potential mechanisms of E during ICP, and can be used as a reference to further improve  
121 hydrological models of alpine lakes.

## 122 **2. Materials and Methods**

### 123 **2.1. Study area**

124 QHL ( $36^{\circ}32'\sim 37^{\circ}15'\text{ N}$ ,  $99^{\circ}36'\sim 100^{\circ}47'\text{ E}$ , 3194 m a.s.l.), with an area of 4,432  $\text{km}^2$  and a catchment of  
125 29,661  $\text{km}^2$ , is the largest inland saline lake in China (Li et al., 2016). The average depth of the lake is  
126 26 m. The average salt content is  $14.13\text{ g L}^{-1}$ , and the pH ranges from 9.15 to 9.30. The hydrochemical  
127 type of the lake water is Na-SO<sub>4</sub>-Cl (Li et al., 2016). Surrounded by mountains, the QHL is a typical  
128 closed tectonic depression lake, which is fed by five major rivers, including the Buha, Shaliu, Hargai,  
129 Quanji, and Heima Rivers (Jin et al., 2015). The total annual water discharge is approximately  $1.56 \times 10^9$

---

130 m<sup>3</sup>, of which the Buha River contributes 50% and Shaliu River contributes approximately one third (Jin  
131 et al., 2015). The mean annual Ta, precipitation, and E values between 1960 and 2015 were −0.1 °C, 355  
132 mm and 925 mm, respectively (Li et al., 2016). The seasonal stratification of QHL corresponded to that  
133 of a dimictic lake with the spring overturn taking place around May and the autumn overturn appearing  
134 around November–December (Su et al., 2019). The ICP usually begins in late November, ends in mid–  
135 late March or even early April, and lasts approximate 100 days. Under the effects of climate warming,  
136 QHL has experienced temperature increases, area expansion, and ICP shortening in the last two decades  
137 (Tang et al., 2018; Han et al., 2021).

## 138 2.2. Site description and energy exchange flux and climate data

139 The instruments to measure the energy exchange flux and micrometeorological parameters were installed  
140 at the China Torpedo Qinghai Lake test base (36°35'27.65" N, 100°30'06" E, 3198 m a.s.l.) located in  
141 the southeastern QHL approximately 737 m from the nearest shore (Li et al., 2016) (Fig. 1). The water  
142 depth underneath this platform is 18 m. The torpedo test tower has a height of 10 m above the water  
143 surface. The EC system was installed on a steel pillar mounted on the northwestern side of the top of the  
144 torpedo test tower with a total height of 17.3 m above the lake water surface (Li et al., 2016). A three–  
145 dimensional sonic anemometer (model CSAT3, Campbell Scientific Inc., Logan, UT, USA) was used to  
146 directly measure horizontal and vertical wind velocity components (u, v, and w) and virtual temperature.  
147 An open–path infrared gas analyzer (model EC150, Campbell Scientific Inc.) was applied to measure  
148 fluctuations in water vapor and carbon dioxide concentrations. Fluxes of sensible heat (H) and latent heat  
149 (LE) were calculated from the 10–Hz time series at 30–min intervals and recorded by a data logger  
150 (CR3000, Campbell Scientific Inc.). The observation instruments were powered by solar energy.

151 A suite of auxiliary micrometeorology was also measured as 30–min averages of 1–s readings on the  
152 eastern side of the top of the torpedo test tower, 3 m from the EC instruments. The net radiation (Rn) was  
153 calculated from the incoming shortwave, reflected shortwave, and incoming and outgoing longwave  
154 radiation, which were measured by a net radiometer (CNR4, Kipp & Zonen B.V., Delft, Netherlands) at  
155 10 m above the lake surface (Fig. 1; Table S1). The Ta, relative humidity (RH), and air pressure (Pres)  
156 were measured at a height of 12.5 m above the water surface (Table S1). A wind sentry unit (model 05103,  
157 RM Young, Inc. Traverse City, MI, USA) was employed to measure the WS and wind direction (WD)

---

158 (Table S1). The  $T_s$  was measured with an infrared thermometer (model SI-111, Campbell Scientific Inc.)  
159 approximately 10 m above the water surface, and the water temperature ( $T_l$ ) was measured with five  
160 temperature probes (109 L, Campbell Scientific Inc.) at depths of 0.2, 0.5, 1.0, 2.0, and 3.0 m.  
161 Precipitation was measured with an automated tipping-bucket rain gauge (model TE525, Campbell  
162 Scientific Inc.) and precipitation gauge (model T-200B, Campbell Scientific Inc.) (Table S1). The  
163 observation system began operation on May 11, 2013. In this study, we unified all observational data at  
164 30-min intervals and analyzed the data from January 1, 2014 to December 31, 2019 (Table S1).

### 165 2.3. Reanalysis climate datasets

166 The reanalysis climate datasets used to drive the lake E models were acquired from the interim reanalysis  
167 dataset v5 (ERA5) produced by the European Centre for Medium-Range Weather Forecasts  
168 (<https://cds.climate.copernicus.eu/cdsapp#!/search?type=dataset>) and the China Regional High-  
169 Temporal-Resolution Surface Meteorological Elements-Driven Dataset (CMFD)  
170 (<http://data.tpdc.ac.cn/en/>). Gridded hourly ERA5 skin temperature and daily WS, daily CMFD  $T_a$ , Pres,  
171 RH, and downward shortwave radiation ( $R_s$ ) at a spatial resolution of  $0.1^\circ$  from 2001 to 2018 were  
172 analyzed in this study (Table S1). The daily skin temperature was generated by averaging the hourly  
173 temperature over 24 h per day and was adopted as the lake surface temperature. We extracted climate  
174 data pertaining to QHL via a grid mask with a spatial resolution of  $0.1^\circ$  and averaged the data in all pixels.  
175 Considering the advantages of long-time spans and high resolution, the ERA5 and CMFD datasets  
176 developed based on land station data have been recognized as the best currently available reanalysis  
177 products and have been widely applied in land-surface and hydrological modeling studies in China (Ma  
178 et al., 2016; Zhu et al., 2016; Tian et al., 2021; Xiao and Cui, 2021). To reduce the uncertainty caused by  
179 the input data, the daily lake surface temperature and WS from ERA5,  $T_a$ ,  $R_s$ , RH, and Pres from CMFD  
180 for QHL were adjusted with fitting equations of the observed daily  $T_s$  ( $R^2 = 0.92$ ,  $P < 0.01$ ), WS ( $R^2 =$   
181  $0.55$ ,  $P < 0.01$ ),  $T_a$  ( $R^2 = 0.90$ ,  $P < 0.01$ ),  $R_s$  ( $R^2 = 0.73$ ,  $P < 0.01$ ), RH ( $R^2 = 0.63$ ,  $P < 0.01$ ), and Pres ( $R^2$   
182  $= 0.95$ ,  $P < 0.01$ ) from 2014 to 2018 (Fig. S1), and the equations are shown below:

$$183 \quad T_a^{ad} = 1.01 \times T_a^{CMFD} + 0.71 \quad (1)$$

$$184 \quad T_s^{ad} = 0.71 \times T_s^{ERA5} + 3.30 \quad (2)$$



---

$$185 \quad R_s^{ad} = 0.86 \times R_s^{CMFD} + 34.63 \quad (3)$$

$$186 \quad WS^{ad} = 0.60 \times WS^{ERA5} + 0.76 \quad (4)$$

$$187 \quad RH^{ad} = 0.68 \times RH^{CMFD} + 19.95 \quad (5)$$

$$188 \quad Pres^{ad} = 0.97 \times Pres^{CMFD} + 30.72 \quad (6)$$

189 Where  $Ta^{ad}$ ,  $Ts^{ad}$ ,  $Rs^{ad}$ ,  $WS^{ad}$ ,  $RH^{ad}$ , and  $Pres^{ad}$  are  $Ta$ ,  $Ts$ ,  $Rs$ ,  $WS$ ,  $RH$ , and  $Pres$  of ERA5 and  
190 CMFD after adjustment, respectively.

#### 191 **2.4. Lake ice coverage dataset and ice phenology**

192 The daily lake ice coverage of QHL from 2002 to 2018 was extracted from a lake ice coverage dataset  
193 of 308 lakes (with an area greater than 3 km<sup>2</sup>) on the QTP retrieved from the National Tibetan Plateau  
194 Data Center (<https://doi.org/10.11922/sciencedb.744>). The dataset with a time span from 2002 to 2018  
195 was generated from the Moderate Resolution Imaging Spectroradiometer (MODIS) normalized  
196 difference snow index (NDSI, with a spatial resolution of 500 m) product with the SNOWMAP algorithm,  
197 and the data under cloud cover conditions were redetermined based on the temporal and spatial continuity  
198 of lake surface conditions (Qiu et al., 2019). Based on the lake ice coverage, the IFP was defined as ice  
199 coverage lower than 10%, and the ICP was defined as ice coverage higher than 10% (Qiu et al., 2019).  
200 The ICP was divided into three stages: freeze (FZ: 10% < ice coverage < 90%), completely freeze (CF:  
201 ice coverage > 90%) and thaw (TW: 10% < ice coverage < 90%) (Qiu et al., 2019). We defined the cycle  
202 year (annual: AN) from the beginning of the IFP to the end of the ICP. This ice coverage has been  
203 compared with that from two other datasets based on passive microwave, and was found to be highly  
204 consistent with each other at an average R<sup>2</sup> of 0.86 and an RMSE of 0.13 in QHL (Qiu et al., 2019). Thus,  
205 this dataset is very accurate and suitable for the division of lake ice phenology in QHL.

#### 206 **2.5 Data processing of the observed energy exchange flux and climate data**

207 The EC fluxes were processed and corrected based on the 10-Hz raw time series data in the data  
208 processing software EdiRe, including spike removal, lag correction of water to carbon dioxide relative  
209 to the vertical wind component, sonic virtual temperature correction, performance of planar fit coordinate  
210 rotation, density fluctuation correction (WPL correction) and frequency response correction (Li et al.,

---

211 2016). Since the shortest distance between the Chinese torpedo Qinghai Lake test base and the  
212 southwestern lakeshore is only 737 m, there may be insufficient fetch for a turbulent flux under certain  
213 conditions. Therefore, footprint analysis was conducted to eliminate data influenced by the surrounding  
214 land. For further details on the process and results of the footprint analysis, see Li et al. (2016). In addition  
215 to these processing steps, quality control of the 30-min flux data was conducted using a five-step  
216 procedure: (i) data originating from periods of sensor malfunction were rejected (e.g., when there was a  
217 faulty diagnostic signal), (ii) data within 1 h before or after precipitation were rejected, (iii) incomplete  
218 30-min data were rejected when the missing data constituted more than 3% of the 30-min raw record,  
219 (iv) data were rejected at night when the friction velocity was below  $0.1 \text{ m s}^{-1}$  (Blanken et al., 1998) and  
220 (v) data with large footprints ( $>700 \text{ m}$ ) and a wind direction from  $180^\circ$  to  $245^\circ$  were eliminated.

221 To further control the quality of the energy exchange flux (sensible heat flux and latent heat flux: H and  
222 LE, respectively) and micrometeorological dataset ( $R_n$ ,  $T_a$ ,  $T_s$ ,  $T_l$ , RH, WS, Pres, and albedo), data  
223 outside the mean  $\pm 3 \times$  standard deviation were removed for each variable. Then, gap-filling methods  
224 entailing a look-up table and mean diurnal variation (Falge et al., 2001) were adopted to fill gaps in the  
225 flux measurement data. The look-up table method was applied when the meteorological dataset was  
226 available synchronously. Otherwise, the mean diurnal variation method was adopted. The heat storage  
227 change ( $G$ ,  $\text{W m}^{-2}$ ) was estimated as a residual of the energy balance:

$$228 \qquad \qquad \qquad G = R_n - LE - H \qquad \qquad \qquad (7)$$

229 where  $R_n$  is the net radiation ( $\text{W m}^{-2}$ ), H is the sensible heat flux ( $\text{W m}^{-2}$ ) and LE is the latent heat flux  
230 ( $\text{W m}^{-2}$ ). Lake E was calculated as

$$231 \qquad \qquad \qquad E = \lambda \times LE \qquad \qquad \qquad (8)$$

232 where  $\lambda$  is the latent heat of vaporization ( $\text{MJ kg}^{-1}$ ), taken as  $2.45 \text{ MJ kg}^{-1}$  in this paper (Allen et al.,  
233 1998).

## 234 **2.6. Models for daily lake evaporation simulation**

235 To evaluate the interannual variation in QHL E from 2003 to 2017, we validated three models during the  
236 AN, IFP, and ICP. Considering that Qinghai Lake is a saline lake, and many studies have pointed out that  
237 it is valuable to consider the influence of salinity on saline lake evaporation, and with the increase of

238 salinity, it will exert greater inhibition on evaporation (Hamdani et al., 2018; Mor et al., 2018). Thus, the  
 239 water activity coefficient ( $\alpha$ ), which is defined as the ratio between the vapor pressure above saline water  
 240 and that above freshwater at the same temperature, has been introduced to characterize the effect of  
 241 salinity on saline lake evaporation (Salhotra et al., 1987; Lensky et al., 2018). Because saline water drains  
 242 out salt during freezing (Badawy, 2016), we only introduced the  $\alpha$  into the evaporation simulation of  
 243 Qinghai Lake during IFP. The three models were as follows:

244 1) Mass-transfer model (MT model) (Harbeck et al., 1958)

$$245 \quad E_{MT} = N \times F(WS) \times \Delta e \quad (9)$$

$$246 \quad F(WS) = a1 \times WS + a2 \quad (10)$$

$$247 \quad \Delta e = \begin{cases} \alpha \times e_s - RH \times e_a & \text{During IFP} \\ e_s - RH \times e_a & \text{During ICP} \end{cases} \quad (11)$$

$$248 \quad e_s = 6.105 \times \exp\left(\frac{17.27 \times Ts}{Ts + 237.7}\right) \quad (12)$$

$$249 \quad e_a = 6.105 \times \exp\left(\frac{17.27 \times Ta}{Ta + 237.7}\right) \quad (13)$$

250 where  $E_{MT}$  is the E rate ( $\text{mm d}^{-1}$ ); N is the mass-transfer coefficient; WS is the wind speed ( $\text{m s}^{-1}$ );  $\Delta e$   
 251 is the vapor pressure difference,  $e_s$  and  $e_a$  are the saturated vapor pressures at the lake surface  
 252 temperature ( $T_s$ ) and air temperature ( $T_a$ ), respectively. And an  $\alpha$  value of 0.97 was suggested for QHL  
 253 during IFP, as measured with a portable water activity meter (AwTester, China). This model inherently  
 254 accounts for the water salinity through  $\Delta e$  and requires calibration of coefficients N, a1, and a2, which  
 255 were taken as 1.26, 0.04, and 0.17 during the AN, respectively; 0.41, 0.17, and 0.28 during the IFP,  
 256 respectively; and 0.90, 0.18, and 0.28, during the ICP, respectively, in this study.

257 2) Atmospheric dynamics model (AD model) (Hamdani et al., 2018)

$$258 \quad E_{AD} = \frac{0.622 \times Ce}{\rho_w \times P} \times \rho_a \times WS \times 3.6 \times 10^6 \times \Delta e \quad (14)$$

$$259 \quad \rho_a = 1.293 \times \left(\frac{273.15}{273.15 + Ta}\right) \times \frac{Pres}{101.325} \quad (15)$$

260 where  $\rho_w$  and  $\rho_a$  denote the water and air densities ( $\text{kg m}^{-3}$ ), respectively, and  $\rho_w$  is approximately  
 261  $1.011 \times 10^3 \text{ kg m}^{-3}$  for QHL. Moreover,  $Pres$  is the air pressure (mbar), and  $Ce$  is a transport

---

262 coefficient obtained via calibration to address missing friction velocity values in the reanalysis climate  
263 datasets, which was taken as  $4.10 \times 10^{-3}$ ,  $3.80 \times 10^{-3}$ , and  $8.40 \times 10^{-3}$  during the AN, IFP, and ICP,  
264 respectively, in this paper.

265 3) Statistical model based on solar radiation (the Jensen–Haise method: JH model) (Wang et al., 2019b)

$$266 \quad E_{JH} = JH1 \times (JH2 \times (T_a - T_s) + JH3) \times (R_s) \times (WS) \quad (16)$$

267 where  $R_s$  is the incoming solar shortwave radiation ( $\text{W m}^{-2}$ ); JH1, JH2, and JH3 must be calibrated  
268 and were taken as 0.06,  $-2.20 \times 10^{-3}$ , and  $5.03 \times 10^{-3}$ , during the AN, respectively; 0.08,  $-2.00 \times 10^{-3}$ ,  
269 and 0.04, during the IFP, respectively; and 0.02,  $7.40 \times 10^{-3}$ , and 0.18, during the ICP, respectively, in  
270 this paper.

271 The three models were selected, first, as they are typical representatives in considering mass transfer,  
272 aerodynamics, and energy transfer; second, because their demand parameters are easy to acquire, which  
273 are adaptive to be promoted; and third, as they have been proven to be efficient in saline lakes (Hamdani  
274 et al., 2018). These models were first calibrated and validated based on daily E observations from 2014  
275 to 2019 during AN, IFP, and ICP, respectively. The root–mean–square error (RMSE) and goodness of fit  
276 ( $R^2$ ) were used to evaluate the effectiveness of the models. A model with high  $R^2$  and low RMSE values  
277 was selected for lake E simulation during the AN, IFP, and ICP.

## 278 **2.7. Statistical analysis**

279 Summer and autumn were taken as June to August and September to November, respectively. During  
280 data analysis, we first divided the 30–min observed energy exchange flux and climate data from 2014 to  
281 2019 by the AN, IFP, and ICP based on the calculated ice phenology. Hence, we obtained datasets of five  
282 cycle years from the IFP in 2014 to the ICP in 2018 (Fig. S2). Second, we calculated the multiday average  
283 30–min energy exchange flux during the IFP and ICP in each year to evaluate the basic statistical  
284 characteristics of the diurnal E and exchange flux. The daily energy exchange flux and climate data were  
285 calculated by averaging the 30–min observed data for each day, the daytime (nighttime) energy exchange  
286 flux and climate data were calculated by averaging the 30–min observed data of 8:00 am to 7:30 pm  
287 (8:00 pm to 7:30 am). And one–way ANOVA was performed to compare the difference in E and G  
288 between the IFP and ICP in each year from 2014 to 2018. Third, to explore the key factor controlling

---

289 lake E, partial least squares regression and random forest methods were used to calculate the sensitivity  
290 coefficient (representing the regression coefficient of each variable, which means the amount of change  
291 in E caused by the variation of per unit in the variable) and importance of Rn, WS,  $\Delta e$ , Pres, albedo, WD,  
292  $T_a - T_s$ , Tl, and ICR to E during the daytime and nighttime of IFP and ICP, respectively. The two methods  
293 analyze the relationship between E and climate and environmental factors from linear and nonlinear  
294 processes, respectively, and have been widely used in the study of hydrological and ecological fields  
295 (Desai and Ouarda, 2021; Li et al., 2022; Sow et al., 2022). Finally, three models were validated and two  
296 models were selected to severally calculate the interannual E during the IFP and ICP from 2003 to 2017  
297 (the available ice phenology exhibits a limited cycle year from 2003 to 2017). Four controlled tests were  
298 then conducted to quantify the contribution of the variation in  $T_a$ ,  $T_s$ , WS, and  $R_s$  to lake E from 2003 to  
299 2017. The analysis of partial least squares regression, random forest methods, and E simulation,  
300 calibration and verification were conducted by daily datasets. The partial least squares and random forest  
301 analyses were conducted in R and the others were conducted in MATLAB.

### 302 **3. Results**

#### 303 **3.1. Diurnal and seasonal characteristics of evaporation and the energy budget during the different** 304 **freeze–thaw periods**

305 The average E, LE, G, H, and Rn values (average from 2014 to 2018) were  $1.20 \pm 0.09 \text{ mm d}^{-1}$ ,  $68.01 \pm$   
306  $4.93 \text{ W m}^{-2}$ ,  $192.18 \pm 7.00 \text{ W m}^{-2}$ ,  $16.25 \pm 1.21 \text{ W m}^{-2}$ , and  $276.45 \pm 3.32 \text{ W m}^{-2}$ , respectively, during  
307 the IFP; and  $1.11 \pm 0.20 \text{ mm d}^{-1}$ ,  $63.15 \pm 11.31 \text{ W m}^{-2}$ ,  $79.23 \pm 18.12 \text{ W m}^{-2}$ ,  $4.68 \pm 0.37 \text{ W m}^{-2}$ , and  
308  $147.06 \pm 14.23 \text{ W m}^{-2}$ , respectively, during the ICP. The daytime E, LE, G, H, and Rn values were notably  
309 lower during the ICP than during the IFP, except for E and LE in 2014 (Figs. 2 and 3; Table S2). In  
310 addition, the daily peak LE and E values typically occurred at approximately 12 pm during the IFP and  
311 approximately 2 pm during the ICP, and exhibited an approximately two–hour lag during the IFP and a  
312 four–hour lag during the ICP over G and Rn (Fig. 2). At night, although lower E (at an average rate of  
313  $0.81 \pm 0.17 \text{ mm d}^{-1}$ ) and LE ( $46.02 \pm 9.71 \text{ W m}^{-2}$ ) levels occurred during the ICP than during the IFP (at  
314 average rates of  $0.94 \pm 0.05 \text{ mm d}^{-1}$  and  $53.09 \pm 2.94 \text{ W m}^{-2}$ , respectively), E (LE) accounted for 42%~45%  
315 and 41%~45% of the total daily E during the IFP and ICP, respectively (Figs. 2 and 3; Table S2).

---

316 Regarding G, a similar release rate was found during IFP and ICP, but the heat release time was longer  
317 during ICP than during IFP (Fig. 2).

318 The daily E ranged from 1.96 to 2.34 mm d<sup>-1</sup> during the IFP and from 1.57 to 2.71 mm d<sup>-1</sup> during the  
319 ICP, and the average E sum reached 593.37 ± 44.87 mm yr<sup>-1</sup> during the IFP and 175.22 ± 45.98 mm yr<sup>-1</sup>  
320 during the ICP from 2014 to 2018 (Figs. 3 and S2; Table S2). This suggested an average E sum of 77%  
321 during the IFP and 23% during the ICP throughout the cycle year from 2014 to 2018 (with a lake E sum  
322 ranging from 719.45 to 798.55 mm yr<sup>-1</sup> and an average value of 768.58 ± 28.73 mm yr<sup>-1</sup>) (Fig. 3). In  
323 terms of G, QHL initially released heat in autumn, which lasted until the lake was completely frozen,  
324 after which heat was absorbed from the lake thawing period throughout the summer (Figs. S2 and S3).

### 325 **3.2. Response of evaporation to climatic factors during the different freeze–thaw periods**

326 The key controlling factor of lake E was explored based on the daily observed energy exchange flux and  
327 climate data (E, Rn, WS, Δe, Pres, albedo, WD, Ta–Ts, and TI) and ICR during the IFP and ICP from  
328 2014 to 2018. The Δe (with a sensitivity coefficient of 0.28 in the daytime and 0.22 in the nighttime, P <  
329 0.05), WS (with a sensitivity coefficient of 0.54 in the daytime and 0.43 in the nighttime, P < 0.05) and  
330 Pres (with a sensitivity coefficient of 0.26 in the daytime and 0.14 in the nighttime, P < 0.05) notably  
331 increased E (Fig. 4), and the effect was greater in the daytime than in the nighttime during the IFP (Fig.  
332 4). The Rn (with a sensitivity coefficient of 0.25 in the nighttime, P < 0.05), WS (with a sensitivity  
333 coefficient of 0.30 in the daytime and 0.22 in the nighttime, P < 0.05), Ta–Ts (with a sensitivity coefficient  
334 of 0.59 in the daytime and 0.39 in the nighttime, P < 0.05) and ICR (with a sensitivity coefficient of 0.20  
335 in the daytime and 0.17 in the nighttime, P < 0.05) imposed a significant positive effect on E during the  
336 ICP (Fig. 4). Similarly, the top five important factors calculated with the random forest method were WS,  
337 Δe, Pres, WD, and Ts during the IFP and Ta–Ts, Ta, WS, Rn, and ICR during the ICP (Fig. S4). This  
338 indicated that E of QHL was mainly controlled by WS, Δe, and Pres during the IFP but was driven by  
339 Rn, Ta–Ts, WS, and ICR during the ICP.

### 340 **3.3. Evaporation simulation and interannual variation**

341 Three models (MT, AD, and JH) were calibrated and validated to evaluate the interannual variation in  
342 QHL E from 2003 to 2017. In the case of model performance, the MT model based on molecular diffusion

---

343 performed the best in terms of E simulation during the IFP (with the largest  $R^2$  and smallest RMSE values  
344 of 0.79 and 0.85, respectively), while the JH model based on energy exchange performed the best during  
345 the ICP (with the largest  $R^2$  and smallest RMSE values of 0.65 and 1.02, respectively) (Figs. S5 and S6).  
346 Thus, the interannual variation in E from 2003 to 2017 was calculated with the MT model during the IFP  
347 and with the JH model during the ICP (Fig. 5). From 2003 to 2017, increases in  $\Delta e$  (at a rate of 0.01 hPa  
348  $\text{yr}^{-1}$ ) and  $T_s$  (at a rate of 0.001  $^{\circ}\text{C yr}^{-1}$ ) resulted in an increase in E (at a rate of 1.62  $\text{mm yr}^{-1}$  for the E  
349 sum) during the IFP (Figs. 5 and S7). Conversely, ignoring the increases in  $T_a$  (at a rate of 0.04  $^{\circ}\text{C yr}^{-1}$ )  
350 and  $T_a - T_s$  (at a rate of 0.04  $^{\circ}\text{C yr}^{-1}$ ), with decreasing WS (at a rate of  $-0.005 \text{ m s}^{-1} \text{ yr}^{-1}$ ), E (at a rate of  
351  $-1.98 \text{ mm yr}^{-1}$  for the E sum) decreased during the ICP, which resulted in an inapparent decrease in E (at  
352 a rate of  $-0.36 \text{ mm yr}^{-1}$  for the E sum) during the AN (Figs. 5 and S7).

## 353 4. Discussion

### 354 4.1. Lake evaporation during the ice-covered period

355 The results of this study highlight the important contribution of lake ice sublimation to the total amount  
356 of lake E. Due to the low snow coverage of Qinghai Lake in winter (with a maximal snow coverage less  
357 than 16% of the area of Qinghai Lake), evaporation and sublimation of lake ice and water are the major  
358 sources of E during the ICP of 2013~2018 (Fig S8). The experimental and simulation results of Jambon–  
359 Puillet et al. (2018) verified that the E rates of liquid droplets and ice crystals remain the same under  
360 unchanged environmental conditions. In this study, the E rate of QHL during the ICP ranged from 1.57  
361 to 2.71  $\text{mm d}^{-1}$ , approximately 0.73~1.38 times that of liquid water during the IFP (Table S2), with similar  
362 results to those findings of liquid droplets and ice crystals. Few studies have examined lake ice E during  
363 the ICP, and most of which have focused on polar sea ice and alpine snow packs (Froyland et al., 2010;  
364 Froyland, 2013; Herrero et al., 2016; Christner et al., 2017; Lin et al., 2020). Observational and modelling  
365 studies of Antarctic ice sheets or lakes have found that the monthly E rate of ice ranged from  $-4.6$  to 13  
366  $\text{mm month}^{-1}$  from June to September (Antarctic) (Froyland et al., 2010). In this study, we found that the  
367 E sum ranges from 130.59 to 262.45  $\text{mm}$  during the ICP (approximately 51.60 to 81.3  $\text{mm month}^{-1}$ , by  
368 multiplying the mean daily E of ICP by 30) from 2014 to 2018, which is higher than the previous  
369 observations from Antarctic ice sheets or lakes. This may be because Antarctic ice sheets or lakes are  
370 located at high latitudes with low solar radiation and are therefore cooler from the surface to greater

---

371 depths with energy-limiting conditions for E (Persson et al., 2002). However, the lakes on the QTP freeze  
372 seasonally, most of these lakes can store a large amount of heat because of the high solar radiation during  
373 the IFP (Fig. 6), which lead to the observed E during the ICP (Huang et al., 2011 and 2016). Studies on  
374 surface E of a shallow thermokarst lake in the central QTP region have found that E reaches up to 250  
375 mm yr<sup>-1</sup> during the ICP (Huang et al., 2016), which is close to our observed E levels (130.59~262.45  
376 mm yr<sup>-1</sup>). Our results further showed that E of QHL accounted for 23% of the annual E during the ICP.  
377 Wang et al. (2020) evaluated 75 large lakes on the QTP and demonstrated that the E of these lakes in  
378 winter accounted for 12.3~23.5% of the annual E, which suggests that E of these lakes during the ICP  
379 was the same as that during the other seasons. Furthermore, considering that the area of QHL is 4,432  
380 km<sup>2</sup> (Li et al., 2016), QHL releases  $3.39 \pm 0.13$  km<sup>3</sup> of water into the air every year, which corresponds  
381 to the sum of the water for animal husbandry, industrial and domestic uses in Qinghai Province (an  
382 average of 2014 to 2017) (Dong et al., 2021).

#### 383 **4.2. Responses of lake evaporation to salinity**

384 Salinity greatly influences the E of saline lakes by changing both water density and thermal properties,  
385 dissolved salt ions can reduce the free energy of water molecules, and result in a higher boiling point and  
386 reduced saturated vapor pressure above saline lakes (Salhotra et al., 1987; Abdelrady, 2013; Mor et al.,  
387 2018). Therefore, an increase in the salinity of a lake would decrease its E rate. For example, Houk (1927)  
388 compared the E of pure water with that of saline lakes of different densities (salinity) in Nevada, USA,  
389 and found that when the density (salinity) of water increased by 1%, the E of saline lakes decreased by  
390 0.01% compared with that of pure water. Similarly, Mor et al. (2018) found that the E rate in diluted  
391 plume is nearly three times larger than that in open lake in the Dead Sea. Thus, the thermodynamic  
392 concept of water activity which is defined as the ratio of water vapor pressure on the surface of saline  
393 and fresh water at the same temperature (the water activity of freshwater is 1, while that of saline water  
394 is lower than 1, and the higher the salinity is, the lower the water activity in lakes) has been widely used  
395 in E simulations of saline lakes (Salhotra et al., 1987; Abdelrady, 2013; Mor et al., 2018). In our study,  
396 we measured the water activity of QHL as 0.97 by a salinity of 14.13 g L<sup>-1</sup>, and applied it to the MT and  
397 AD models for E simulation of IFP during 2003 to 2017, which make it more theoretical to explain the  
398 E process of saline lakes and reduced the uncertainty of estimation in saline lake E. For example, with



---

399 the salinity of  $133 \text{ g L}^{-1}$  of surface water, water activity was measured to be 0.65, and has been widely  
400 used in its E simulation of the Dead Sea (Metzger et al., 2018; Mor et al., 2018; Lensky et al., 2018); and  
401 Abdelrady (2013) improved the surface energy balance system (SEBS) of E in saline lakes by  
402 constructing an exponential function between lake salinity and water activity, which reduced the  
403 simulated E by 27% and RMSE from  $0.62$  to  $0.24 \text{ mm (3h)}^{-1}$  in Great Salt Lake. Therefore, considering  
404 salinity is essential to enhance the accuracy of E simulations in saline lakes.

### 405 **4.3. Responses of lake evaporation to climate variability**

406 In addition, climate and environment are also important factors affecting lake E and vary significantly  
407 between the different seasons. Previous studies have shown that lake E is mostly affected by WS and  $\Delta e$   
408 in summer and WS,  $\Delta e$ ,  $T_a - T_s$ , and G in winter (Zhang and Liu, 2014; Hamdani, et al., 2018). This  
409 suggests that energy exchange between lakes and air may be one of the main drivers of E during the ICP  
410 under the same atmospheric boundary conditions (Fig. 6). Since most lakes store heat in summer, they  
411 release heat and sufficiently produce E in winter (Blanken et al., 2011; Hamdani, et al., 2018). In this  
412 study, we also found that QHL began to store heat in the lake thawing period and released heat in autumn  
413 or when the lake began to freeze (Figs. 6 and S3). Therefore, E of QHL was mostly controlled by WS,  
414  $\Delta e$ , and Pres during the IFP, whereas it was mainly affected by Rn,  $T_a - T_s$ , and WS during the ICP (Fig.  
415 6).

416 Furthermore, the QTP has been suffering surface air warming and moistening, solar dimming, and wind  
417 stilling since the beginning of the 1980s across the QTP (Yang et al., 2014; Kuang and Jiao, 2016), which  
418 affects the hydrothermal processes of the lake, such as increasing  $T_s$  and shortening lake ice phenology  
419 (Wan et al., 2018; Cai et al., 2019). An increase in  $T_s$  enhances the diffusion of water molecules and  
420 enlarges  $\Delta e$  between the water surface and the air, which in turn promotes evaporation (Wang et al., 2018;  
421 Woolway et al., 2020), while a reduction in solar radiation decreases the energy input of the lake, and  
422 wind stilling enhances the stability of the atmosphere above the water surface, which in turn inhibits  
423 evaporation (Roderick and Farquhar, 2022; Guo et al., 2019). We found a decrease in E during the AN  
424 from 2003 to 2017, due to the steeper decrease in E caused by solar dimming and wind stilling during  
425 the ICP than the increase engendered by the increase in  $T_s$  during the IFP. From 2003 to 2017, E decreased  
426 at an average rate of  $-6.48 \pm 4.77 \text{ mm yr}^{-1}$  (3.23%) and  $-11.17 \pm 14.29 \text{ mm yr}^{-1}$  (7.56%) due to decrease

---

427 in Rs and WS during the ICP, respectively (Fig. 7; Table S3), while the increase in Ts increased E at an  
428 average rate of  $13.58 \pm 20.75 \text{ mm yr}^{-1}$  (3.54%) during the IFP (Fig. 7; Table S3). Previous studies have  
429 found similar results in Selin Co and Namu Co (Zhu et al., 2016; Guo et al., 2019). For example, Guo et  
430 al. (2019) found that E was mainly controlled by WS, and a decrease in WS led to a decrease in E from  
431 1985 to 2016 in Selin Co.

432 In addition, changes in lake ice phenology significantly affected lake E during the IFP and ICP. Compared  
433 with 2003 to 2007 ( $101.40 \pm 7.00 \text{ d}$ ), the average ICP decreased by 10.8 d from 2013 to 2017 ( $90.60 \pm$   
434  $6.08 \text{ d}$ ) (Table S3). A shortened ICP suggests a much lower albedo in the cycle year and could result in  
435 higher Rs absorption and a shorter period for heat-induced recession, which could increase lake E (Wang  
436 et al., 2018). Furthermore, lake E is also affected by the lake area, water level, and physical and chemical  
437 properties (Woolway et al., 2020), especially for saline lakes (Salhotra et al., 1987; Mohammed and  
438 Tarboton, 2012; Mor et al., 2018). Increasing the water salinity could reduce E (Salhotra et al., 1987;  
439 Mor et al., 2018) because the dissolved salt ions could reduce the free energy of water molecules (i.e.,  
440 reduced water activity) and result in a lower saturated vapor pressure above saline lakes at a given water  
441 temperature (Salhotra et al., 1987; Mor et al., 2018). However, the changes in lake physical and chemical  
442 properties attributed to lake freezing increase the complexity of the underlying mechanism, simulation  
443 of ice E and its response to climate change, and more studies are needed to further explore interactions  
444 between the different factors.

#### 445 **4.4. Limitation**

446 Based on six continuous year-round direct measurements of lake E and energy exchange flux, we  
447 determined the E loss during the ICP and calibrated and verified different models for E simulation during  
448 the IFP and ICP. Due to the lack of accurate measurements of deep lake temperatures, energy budget  
449 closure ratios of EC observations in QHL are not given in this study. EC measurements have been widely  
450 used to quantify the E of several global lakes, including Lake Superior in America, Great Slave Lake in  
451 Canada, Lake Geneva in Switzerland, Lake Valkea-Kotinen in Finland, and Taihu Lake, Erhai Lake,  
452 Poyang Lake, Nam Co, Selin Co and Ngoring Lake in China (Blanken et al., 2000; Vercauteren et al.,  
453 2009; Blanken et al., 2011; Nordbo et al., 2011; Wang et al., 2014; Li et al., 2015; Liu et al., 2015; Guo  
454 et al., 2016; Li et al., 2016; Ma et al., 2016; Lensky et al., 2018). With most of the known energy budget

---

455 closure ratios over 0.7, EC observations of lakes are regarded as an accurate and reliable direct  
456 measurement method of E, even in lakes over the QTP (Wang et al., 2020). Moreover, compared with  
457 land stations, the energy budget closure ratios over lake surfaces can be significantly influenced by the  
458 large amount of heat storage (release) during different seasons (Wang et al., 2020), which would increase  
459 the uncertainty about the quantification of E. In addition, quantification of E during the ICP depends on  
460 accurate ice phenology identification, and a longer ICP suggests more E. Therefore, the different data  
461 sources and phenological classification methods of ice phenology comprise one source of uncertainty.  
462 Moreover, lake salinity changes dynamically at diurnal, seasonal and interannual scales, but due to the  
463 difficulty of continuously observing lake salinity, the fixed water activity in our study may cause the  
464 underestimation in E of QHL due to the decrease in salinity by the expansion of QHL. Furthermore, in  
465 addition to the traditional lake evaporation models (Dalton formula series, energy and water balance  
466 formula series, Penman formula series, and empirical formula based on statistical analysis), the 1D lake  
467 thermodynamics model has been widely used for the simulation of lake ice thickness and energy balance  
468 (ice sublimation) in ICP (Pour et al., 2017; Stepanenko et al., 2019; Xie et al., 2023). Considering that  
469 this study was concentrated on verifying the consistency of the accuracy of the traditional models for the  
470 evaporation simulation during IFP and ICP. Thus, this study ignored the 1D lake thermodynamics model  
471 for ice sublimation. It is suggested to build the observation system of lake thermodynamics parameters,  
472 verify and develop a suitable 1D or even 3D lake thermodynamics evaporation models for QHL in future  
473 study.

## 474 **5. Conclusions**

475 In summary, based on six continuous year-round 30-min direct flux measurements throughout the cycle  
476 year from 2014 to 2018, the night E of QHL occupied over 40% during both the IFP and ICP. With a  
477 multiyear average of  $175.22 \pm 45.98 \text{ mm yr}^{-1}$ , E during the ICP accounted for 23% of the total cycle year  
478 E sum, which is an important component in calculating the E of saline lakes. A difference-based control  
479 factor of E was also found during the IFP and ICP. E of QHL was mainly controlled by atmospheric  
480 dynamic factors (WS,  $\Delta e$ , and P) during the IFP, whereas it was driven by both energy exchange and  
481 atmospheric boundary conditions ( $R_n$ ,  $T_a - T_s$ , and WS) during the ICP. Thus, the MT model based on  
482 molecular diffusion performed best in lake E simulation during the IFP, while the JH model based on

---

483 energy exchange performed best during the ICP. Furthermore, simulation of the E of QHL showed a  
484 slight decrease from 2003 to 2017, caused by a decrease in E during the ICP, and WS weakening may  
485 have resulted in an average reduction of 7.56% in lake E during the ICP from 2003 to 2017. Our results  
486 suggest that E during the ICP is non-negligible for saline lake E, and E simulation should be further  
487 improved in future model simulation studies, considering the difference in its potential mechanisms  
488 during the ICP.

#### 489 **Code availability**

490 The code of data analysis and plotting are available on the [https://github.com/Clocks-Shi/Code-](https://github.com/Clocks-Shi/Code-for-hess-2023-100)  
491 [for-hess-2023-100](https://github.com/Clocks-Shi/Code-for-hess-2023-100), and also available from the corresponding author upon reasonable request  
492 ([xyli@bnu.edu.cn](mailto:xyli@bnu.edu.cn)).

#### 493 **Data availability**

494 The gridded climate datasets from the interim reanalysis dataset v5 (ERA5) produced by the  
495 European Centre for Medium-Range Weather Forecasts  
496 (<https://cds.climate.copernicus.eu/cdsapp#!/search?type=dataset>) and the China Regional High-  
497 Temporal-Resolution Surface Meteorological Elements-Driven Dataset (CMFD)  
498 (<http://data.tpsc.ac.cn/en/>) can be freely accessed. The daily lake ice coverage data were  
499 retrieved from the National Tibetan Plateau Data Center  
500 (<https://doi.org/10.11922/sciencedb.744>). The observed datasets (energy exchange flux,  
501 meteorological data, hydrochemical parameters) that support the findings of this study are  
502 available from the corresponding author upon reasonable request ([xyli@bnu.edu.cn](mailto:xyli@bnu.edu.cn)).

#### 503 **Author Contributions**

504 XY Li conceived the idea, and FZ Shi performed the analyses. XY Li, FZ Shi, DL Chen, and YJ Ma led  
505 the manuscript writing. SJ Zhao, YJ Ma, JQ Wei, and QW Liao provided analysis of datasets. All authors  
506 contributed to the review and the revision of the manuscript.

#### 507 **Competing interests**

508 The authors declare that they have no known competing financial interests or personal relationships

---

509 that could have appeared to influence the work reported in this paper.

510 **Acknowledgements**

511 The study was financially supported by the National Natural Science Foundation of China  
512 (NSFC: 41971029), the Second Tibetan Plateau Scientific Expedition and Research Program  
513 (STEP: 2019QZKK0306), the State Key Laboratory of Earth Surface Processes and Resource  
514 Ecology (2021-ZD-03), the Ten Thousand Talent Program for Leading Young Scientists and  
515 the China Scholarship Council, the China Postdoctoral Science Foundation (2023M730281),  
516 and the State Key Laboratory of Earth Surface Processes and Resource Ecology of Beijing  
517 Normal University (2023-KF-07).

519 **References**

- 520 Abdelrady, A. R.: Evaporation over fresh and saline water using SEBS. Master's Thesis. University of  
521 Twente, 2013.
- 522 Allen, R. G., Pereira, L. S., Raes, D., and Smith, M.: Crop evapotranspiration—Guidelines for computing  
523 crop water requirements—FAO Irrigation and drainage paper 56, Fao., Rome., 300(9), D05109, 1998.
- 524 Badawy, S. M.: Laboratory freezing desalination of seawater, *Desalin. Water. Treat.*, 57(24), 11040-  
525 11047, <https://doi.org/10.1080/19443994.2015.1041163>, 2016.
- 526 Blanken, P. D., Den Hartog, G., Staebler, R. F., Chen, W. J., and Novak, M.: Turbulent flux measurements  
527 above and below the overstory of a boreal aspen forest, *Bound-Lay. Meteorol.*, 89(1), 109–140,  
528 <https://doi.org/10.1023/A:1001557022310>, 1998.
- 529 Blanken, P. D., Rouse, W. R., Culf, A. D., Spence, C., Boudreau, L. D., Jasper, J. N., Kochtubajda, B.,  
530 Schertzer, W. M., Marsh, P., and Verseghy, D.: Eddy covariance measurements of evaporation from Great  
531 Slave lake, Northwest Territories, Canada, *Water. Resour. Res.*, 36(4), 1069–1077,  
532 <https://10.1029/1999WR900338>, 2000.
- 533 Blanken, P. D., Spence, C., Hedstrom, N., and Lenters, J. D.: Evaporation from Lake Superior: 1. Physical  
534 controls and processes, *J. Great. Lakes. Res.*, 37(4), 707–716, <https://doi.org/10.1016/j.jglr.2011.08.009>,  
535 2011.
- 536 Bowen, I. S.: The ratio of heat losses by conduction and by evaporation from any water surface, *Phys.*  
537 *Rev.*, 27(6), 779, <https://doi.org/10.1103/PhysRev.27.779>, 1926.
- 538 Cai, Y., Ke, C. Q., Li, X., Zhang, G., Duan, Z., and Lee, H.: Variations of lake ice phenology on the  
539 Tibetan Plateau from 2001 to 2017 based on MODIS data, *J. Geophys. Res–Atmos.*, 124(2), 825–843,  
540 <https://doi.org/10.1029/2018JD028993>, 2019.
- 541 Christner, E., Kohler, M., and Schneider, M.: The influence of snow sublimation and meltwater  
542 evaporation on  $\delta D$  of water vapor in the atmospheric boundary layer of central Europe, *Atmos. Chem.*  
543 *Phys.*, 17(2), 1207–1225, <https://doi.org/10.5194/acp-17-1207-2017>, 2017.
- 544 Dalton, J.: Experimental essays on the constitution of mixed gases; on the force of stream or vapor from  
545 water and other liquids, both in a Torricellian vacuum and in air; on evaporation; and on the expansion  
546 of gases by heat, *Proceedings of Manchester Literary and Philosophica Society*, 5, 536–602, 1802.
- 547 Desai, S., and Ouarda, T. B. M. J.: Regional hydrological frequency analysis at ungauged sites with  
548 random, *J. Hydrol.*, 594(3), 125861, <https://doi.org/10.1016/j.jhydrol.2020.125861>, 2021.
- 549 Dong, H., Feng, Z., Yang, Y., Li, P., and You, Z.: Sustainability assessment of critical natural capital: a  
550 case study of water resources in Qinghai Province, China, *J. Clean. Prod.*, 286, 125532,  
551 <https://doi.org/10.1016/j.jclepro.2020.125532>, 2021.
- 552 Falge, E., Baldocchi, D., Olson, R., Anthoni, P., Aubinet, M., Bernhofer, C., Burba, G., Ceulemans, R.,  
553 Clement, R., Dolman, H., Granier, A., Gross, P., Grünwald, P., Hollinger, D., Jensen, N. O., Katul, G. G.,

---

554 Keronen, P., Kowalski, A., Lai, C. T., Law, B. E., Meyers, T., Moncrieff, J., Moors, E., Munger, J. W.,  
555 Pilegaard, K., Rannik, U., Rebmann, C., Suyker, A. E., Tenhunen, J., Tu, K., Verma, S., Vesala, T., Wilson,  
556 K., and Wofsy, S. C.: Gap filling strategies for defensible annual sums of net ecosystem exchange, *Agr.*  
557 *Forest. Meteorol.*, 107(1), 43–69, [https://doi.org/10.1016/S0168-1923\(00\)00225-2](https://doi.org/10.1016/S0168-1923(00)00225-2), 2001.

558 Finch, J., and Calver, A.: Methods for the quantification of evaporation from lakes, Prepared for the  
559 World Meteorological Organization’s Commission for Hydrology, CEH Wallingford, Oxfordshire, UK,  
560 1–41, 2008.

561 Froyland, H. K., Untersteiner, N., Town, M. S., and Warren, S. G.: Evaporation from Arctic sea ice in  
562 summer during the International Geophysical Year, 1957–1958, *J. Geophys. Res–Atmos.*, 115, D15104,  
563 <https://doi.org/10.1029/2009JD012769>, 2010.

564 Froyland, H. K.: Snow loss on the San Francisco peaks: Effects of an elevation gradient on evapo–  
565 sublimation, Doctoral dissertation, Northern Arizona University, 2013.

566 Gross, M.: The world’s vanishing lakes, *Curr. Biol.*, 27(2), 43–46,  
567 <https://doi.org/10.1016/j.cub.2017.01.008>, 2017.

568 Guo, Y., Zhang, Y., Ma, N., Song, H., and Gao, H.: Quantifying surface energy fluxes and evaporation  
569 over a significant expanding endorheic lake in the central Tibetan Plateau, *J. Meteorol. Soc. Jpn. Ser. II*,  
570 94(5), 453–465, <https://doi.org/10.2151/jmsj.2016-023>, 2016.

571 Guo, Y., Zhang, Y., Ma, N., Xu, J., and Zhang, T.: Long–term changes in evaporation over Siling Co  
572 Lake on the Tibetan Plateau and its impact on recent rapid lake expansion, *Atmos. Res.*, 216, 141–150,  
573 <https://doi.org/10.1016/j.atmosres.2018.10.006>, 2019.

574 Hamdani, I., Assouline, S., Tanny, J., Lensky, I. M., Gertman, I., Mor, Z., and Lensky, N. G.: Seasonal  
575 and diurnal evaporation from a deep hypersaline lake: The Dead Sea as a case study, *J. Hydrol.*, 562,  
576 155–167, <https://doi.org/10.1016/j.jhydrol.2018.04.057>, 2018.

577 Han, W. X., Huang, C. L., Gu, J., Hou, J. L., and Zhang, Y.: Spatial–Temporal Distribution of the Freeze–  
578 Thaw Cycle of the Largest Lake (Qinghai Lake) in China Based on Machine Learning and MODIS from  
579 2000 to 2020, *Remote. Sens.*, 13(9), 1695, <https://doi.org/10.3390/rs13091695>, 2021.

580 Harbeck, G. E. Kohler, M. A., and Koberg, G. E.: Water–loss investigations: Lake Mead studies, edited  
581 by: Nolan, T. B., United States Government Printing Office, Washington, <https://doi.org/10.3133/pp298>,  
582 1958

583 Herrero, J., and Polo, M. J.: Evaposublimation from the snow in the Mediterranean mountains of Sierra  
584 Nevada (Spain), *Cryosphere.*, 10(6), 2981–2998, <https://doi.org/10.5194/tc-10-2981-2016>, 2016.

585 Houk, I. E.: Evaporation on United States Reclamation Projects, *Trans. Am. Soc. Civil Eng.*, 90, 340–343,  
586 <https://doi.org/10.1061/TACEAT.0003691>, 1927.

587 Huang, L., Liu, J., Shao, Q., and Liu, R.: Changing inland lakes responding to climate warming in  
588 Northeastern Tibetan Plateau, *Climatic. Change.*, 109(3), 479–502, [https://doi.org/10.1007/s10584-011-](https://doi.org/10.1007/s10584-011-0032-x)  
589 0032-x, 2011.

590 Huang, W., Li, R., Han, H., Niu, F., Wu, Q., and Wang, W.: Ice processes and surface ablation in a shallow

---

591 thermokarst lake in the central Qinghai–Tibetan Plateau, *Ann. Glaciol.*, 57(71), 20–28,  
592 <https://doi.org/10.3189/2016AoG71A016>, 2016.

593 Jambon–Puillet, E., Shahidzadeh, N., and Bonn, D.: Singular sublimation of ice and snow crystals, *Nat.*  
594 *Commun.*, 9(1), 1–6, <https://doi.org/10.1038/s41467-018-06689-x>, 2018.

595 Jin, Z. D., An, Z. S., Yu, J. M., Li, F. C., and Zhang, F.: Lake Qinghai sediment geochemistry linked to  
596 hydroclimate variability since the last glacial, *Quaternary. Sci. Rev.*, 122, 63–73,  
597 <https://doi.org/10.1016/j.quascirev.2015.05.015>, 2015.

598 Kuang, X., and Jiao, J. J.: Review on climate change on the Tibetan Plateau during the last half century,  
599 *J. Geophys. Res–Atmos.*, 121(8), 3979–4007, <https://doi.org/10.1002/2015JD024728>, 2016.

600 Lensky, N. G., Lensky, I. M., Peretz, A., Gertman, I., Tanny, J., and Assouline, S.: Diurnal Course of  
601 evaporation from the dead sea in summer: A distinct double peak induced by solar radiation and night  
602 sea breeze, *Water. Resour. Res.*, 54(1), 150–160, <https://doi.org/10.1002/2017WR021536>, 2018.

603 Li, B., Zhang, J., Yu, Z., Liang, Z., Chen, L., and Acharya, K.: Climate change driven water budget  
604 dynamics of a Tibetan inland lake, *Global. Planet. Change.*, 150, 70–80,  
605 <https://doi.org/10.1016/j.gloplacha.2017.02.003>, 2017.

606 Li, X. Y., Ma, Y. J., Huang, Y. M., Hu, X., Wu, X. C., Wang, P., Li, G. Y., Zhang, S. Y., Wu, H. W., Jiang,  
607 Z. Y., Cui, B. L., and Liu, L.: Evaporation and surface energy budget over the largest high-altitude saline  
608 lake on the Qinghai-Tibet Plateau, *J. Geophys. Res–Atmos.*, 121(18), 10–470,  
609 <https://doi.org/10.1002/2016JD025027>, 2016.

610 Li, X. Y., Shi, F. Z., Ma, Y. J., Zhao, S. J., and Wei, J. Q.: Significant winter CO<sub>2</sub> uptake by saline lakes  
611 on the Qinghai–Tibet Plateau, *Global. Change. Biol.*, 2022, 28(6), 2041–2052,  
612 <https://doi.org/10.1111/gcb.16054>, 2022.

613 Li, Z., Lyu, S., Ao, Y., Wen, L., Zhao, L., and Wang, S.: Long-term energy flux and radiation balance  
614 observations over lake Ngoring, Tibetan Plateau, *Atmos. Res.*, 155, 13–25,  
615 <https://doi.org/10.1016/j.atmosres.2014.11.019>, 2015.

616 Lin, Y., Cai, T., and Ju, C.: Snow evaporation characteristics related to melting period in a forested  
617 permafrost region, *Environ. Eng. Manag. J.*, 19(3), 531–542, <https://doi.org/10.30638/eemj.2020.051>,  
618 2020.

619 Liu, C., Zhu, L. P., Wang, J. B., Ju, J. T., Ma, Q. F., Qiao, B. J., Wang, Y., Xu, T., Hao, C., Kou, Q. Q.,  
620 Zhang, R., and Kai, J. L.: In-situ water quality investigation of the lakes on the Tibetan Plateau, *Sci.*  
621 *Bull.*, 66(17). 1727–1730, <https://doi.org/10.1016/j.scib.2021.04.024>, 2021.

622 Liu, H., Feng, J., Sun, J., Wang, L., and Xu, A.: Eddy covariance measurements of water vapor and CO<sub>2</sub>  
623 fluxes above the Erhai Lake, *Sci. China. Earth. Sci.*, 58(3), 317–328, <https://doi.org/10.1007/s11430-014-4828-1>, 2015.

625 Ma, N., Szilagyi, J., Niu, G. Y., Zhang, Y., Zhang, T., Wang, B., and Wu, Y.: Evaporation variability of  
626 Nam Co Lake in the Tibetan Plateau and its role in recent rapid lake expansion, *J. Hydrol.*, 537, 27–35,  
627 <https://doi.org/10.1016/j.jhydrol.2016.03.030>, 2016.



---

628 Messenger, M. L., Lehner, B., Grill, G., Nedeva, I., and Schmitt, O.: Estimating the volume and age of  
629 water stored in global lakes using a geo-statistical approach, *Nat. Commun.*, 7(1), 13603,  
630 <https://doi.org/10.1038/ncomms13603>, 2016.

631 Metzger, J., Nied, M., Corsmeier, U., Kleffmann, J., and Kottmeier, C.: Dead Sea evaporation by eddy  
632 covariance measurements vs. aerodynamic, energy budget, Priestley–Taylor, and Penman estimates,  
633 *Hydrol. Earth Sys. Sci.*, 22(2), 1135–1155, <https://doi.org/10.5194/hess-22-1135-2018>, 2018.

634 Mohammed, I. N., and Tarboton, D. G.: An examination of the sensitivity of the Great Salt Lake to  
635 changes in inputs, *Water. Resour. Res.*, 48(11), W11511, <https://doi.org/10.1029/2012wr011908>, 2012.

636 Mor, Z., Assouline, S., Tanny, J., Lensky, I. M., and Lensky, N. G.: Effect of water surface salinity on  
637 evaporation: The case of a diluted buoyant plume over the Dead Sea, *Water. Resour. Res.*, 54(3), 1460–  
638 1475, <https://doi.org/10.1002/2017WR021995>, 2018.

639 Nordbo, A., Launiainen, S., Mammarella, I., Leppäranta, M., Huotari, J., Ojala, A., and Vesala, T.:  
640 Long-term energy flux measurements and energy balance over a small boreal lake using eddy covariance  
641 technique, *J. Geophys. Res–Atmos.*, 116, D02119, <https://doi.org/10.1029/2010JD014542>, 2011.

642 Obiany, J. I.: Effect of Salinity on Evaporation and the Water Cycle, *Emerging Science Journal*, 3(4),  
643 256–262, <https://doi.org/10.28991/esj-2019-01188>, 2019.

644 Penman, H. L.: Natural evaporation from open water, bare soil and grass, *P. Roy. Soc. A–Math. Phys.*,  
645 193(1032), 120–145, <https://doi.org/10.1098/rspa.1948.0037>, 1948.

646 Persson, P. O. G., Fairall, C. W., Andreas, E. L., Guest, P. S., and Perovich, D. K.: Measurements near  
647 the Atmospheric Surface Flux Group tower at SHEBA: Near-surface conditions and surface energy  
648 budget, *J. Geophys. Res–Oceans.*, 107(10), 8045, <https://doi.org/10.1029/2000JC000705>, 2002.

649 Pour, H. K., Duguay, C. R., Scott, K. A., and Kang, K. K.: Improvement of lake ice thickness retrieval  
650 from MODIS satellite data using a thermodynamic model, *IEEE. T. Geosci. Remote.*, 55(10), 5956–5965,  
651 <https://doi.org/10.1109/TGRS.2017.2718533>, 2017.

652 Qiu, Y., Xie, P., Leppäranta, M., Wang, X., Lemmetyinen, J., Lin, H., and Shi, L.: MODIS-based daily  
653 lake ice extent and coverage dataset for Tibetan Plateau, *Big Earth Data*, 3(2), 170–185,  
654 <https://doi.org/10.1080/20964471.2019.1631729>, 2019.

655 Roderick M.L. and Farquhar, G.D.: The cause of decreased pan evaporation over the past 50 years,  
656 *Science.*, 298(5597), 1410–1411, <https://doi.org/10.1126/science.1075390-a>, 2002.

657 Salhotra, A. M., Adams, E. E., and Harleman, D. R.: Effect of Salinity and Ionic Composition on  
658 Evaporation: Analysis of Dead Sea Evaporation Pans, *Water. Resour. Res.*, 21(9), 1336–1344,  
659 <https://doi.org/10.1029/WR021i009p01336>, 1985.

660 Salhotra, A. M., Adams, E. E., and Harleman, D. R.: The alpha, beta, gamma of evaporation from saline  
661 water bodies, *Water. Resour. Res.*, 23(9), 1769–1774, <https://doi.org/10.1029/WR023i009p01769>, 1987.

662 Sow, A., Traore, I., Diallo, T., Traore, M., and Ba, A.: Comparison of Gaussian process regression, partial  
663 least squares, random forest and support vector machines for a near infrared calibration of paracetamol  
664 samples, *Results in Chemistry*, 4(3), 100508, <https://doi.org/10.1016/j.rechem.2022.100508>, 2022.

- 
- 665 Stepanenko, V. M., Repina, I. A., Ganbat, G., and Davaa, G.: Numerical simulation of ice cover of saline  
666 lakes, *Izvestiya, Izv. Atmos. Oceanic Phy+.*, 55(1), 129-138, <https://doi.org/10.31857/S0002-3515551152-163>, 2019.
- 668 Su, D. S., Hu, X. Q., Wen, L. J., Lyu, S. H., Gao, X. Q., Zhao, L., Li, Z. G., Du, J., and Kirillin, G.:  
669 Numerical study on the response of the largest lake in China to climate change, *Hydrol. Earth. Sys. Sci.*,  
670 23(4), 2093–2109, <https://doi.org/10.5194/hess-23-2093-2019>, 2019.
- 671 Tang, L. Y., Duan, X. F., Kong, F. J., Zhang, F., Zheng, Y. F., Li, Z., Mei, Y., Zhao, Y. W., and Hu, S. J.:  
672 Influences of climate change on area variation of Qinghai Lake on Qinghai–Tibetan Plateau since 1980s,  
673 *Sci. Rep.*, 8(1), 7331–7338, <https://doi.org/10.1038/s41598-018-25683-3>, 2018.
- 674 Tian, W., Liu, X., Wang, K., Bai, P., and Liu, C.: Estimation of reservoir evaporation losses for China, *J.*  
675 *Hydrol.*, 596(26), 126142, <https://doi.org/10.1016/j.jhydrol.2021.126142>, 2021.
- 676 Vercauteren, N., Bou–Zeid, E., Huwald, H., Parlange, M. B., and Brutsaert, W.: Estimation of wet surface  
677 evaporation from sensible heat flux measurements, *Water. Resour. Res.*, 45(6), W06424, <https://doi.org/10.1029/2008WR007544>, 2009.
- 679 Wan, W., Zhao, L., Xie, H., Liu, B., Li, H., Cui, Y., Ma, Y., and Hong, Y.: Lake surface water temperature  
680 change over the Tibetan plateau from 2001 to 2015: A sensitive indicator of the warming climate,  
681 *Geophys. Res. Lett.*, 45(6), 11–177, <https://doi.org/10.1029/2018GL078601>, 2018.
- 682 Wang, B., Ma, Y., Chen, X., Ma, W., Su, Z., and Menenti, M.: Observation and simulation of lake-air  
683 heat and water transfer processes in a high-altitude shallow lake on the Tibetan Plateau, *J. Geophys. Res–*  
684 *Atmos.*, 120(24), 12327–12344, <https://doi.org/10.1002/2015JD023863>, 2015.
- 685 Wang, B., Ma, Y., Ma, W., Su, B., and Dong, X.: Evaluation of ten methods for estimating evaporation  
686 in a small high–elevation lake on the Tibetan Plateau, *Theor. Appl. Climatol.*, 136(1), 1033–1045,  
687 <https://doi.org/10.1007/s00704-018-2539-9>, 2019b.
- 688 Wang, B., Ma, Y., Su, Z., Wang, Y., and Ma, W.: Quantifying the evaporation amounts of 75 high–  
689 elevation large dimictic lakes on the Tibetan Plateau, *Sci. Adv.*, 6(26), eaay8558,  
690 <https://doi.org/10.1126/sciadv.aay8558>, 2020.
- 691 Wang, B., Ma, Y., Wang, Y., Su, Z., and Ma, W.: Significant differences exist in lake–atmosphere  
692 interactions and the evaporation rates of high–elevation small and large lakes, *J. Hydrol.*, 573, 220–234,  
693 <https://doi.org/10.1016/j.jhydrol.2019.03.066>, 2019a.
- 694 Wang, W., Lee, X., Xiao, W., Liu, S., Schultz, N., Wang, Y., Zhang, M., and Zhao, L.: Global lake  
695 evaporation accelerated by changes in surface energy allocation in a warmer climate, *Nat. Geosci.*, 11(6),  
696 410–414, <https://doi.org/10.1038/s41561-018-0114-8>, 2018.
- 697 Wang, W., Xiao, W., Cao, C., Gao, Z. Q., Hu, Z. H., Liu, S. D., Shen, S. H., Wang, L. L., Xiao, Q. T., Xu,  
698 J. P., Yang, D., and Lee, X. H.: Temporal and spatial variations in radiation and energy balance across a  
699 large freshwater lake in China, *J. Hydrol.*, 511(3–4), 811–824,  
700 <https://doi.org/10.1016/j.jhydrol.2014.02.012>, 2014.
- 701 Woolway, R. I., Kraemer, B. M., Lenters, J. D., Merchant, C. J., O’Reilly, C. M., and Sharma, S.: Global  
702 lake responses to climate change, *Nat. Rev. Earth. Env.*, 1(8), 388–403, <https://doi.org/10.1038/s43017->

---

703 020-0067-5, 2020.

704 Woolway, R. I., Verburg, P., Lenters, J. D., Merchant, C. J., Hamilton, D. P., Brookes, J., De Eyto, E.,  
705 Kelly, S., Healey, N. C., Hook, S., Laas, A., Pierson, D., Rusak, J. A., Kuha, J., Karjalainen, J. S., Kallio,  
706 K., Lepistö, A., and Jones, I. D.: Geographic and temporal variations in turbulent heat loss from lakes: A  
707 global analysis across 45 lakes, *Limnol. Oceanogr.*, 63(6), 2436–2449, <https://doi.org/10.1002/lno.10950>,  
708 2018.

709 Wu, H. W., Huang, Q., Fu, C. S., Song, F., Liu, J. Z., and Li, J.: Stable isotope signatures of river and  
710 lake water from Poyang Lake, China: Implications for river–lake interactions, *J. Hydrol.*, 592, 125619,  
711 <https://doi.org/10.1016/j.jhydrol.2020.125619>, 2021.

712 Wu, H. W., Song, F., Li, J., Zhou, Y. Q., Zhang, J. M., and Fu, C. S.: Surface water isoscapes ( $\delta^{18}\text{O}$  and  
713  $\delta^2\text{H}$ ) reveal dual effects of damming and drought on the Yangtze River water cycles, *J. Hydrol.*, 610(4),  
714 127847, <https://doi.org/10.1016/j.jhydrol.2022.127847>, 2022.

715 Wurtsbaugh, W. A., Miller, C., Null, S. E., DeRose, R. J., Wilcock, P., Hahnenberger, M., Howe, F. P.,  
716 and Moore, J.: Decline of the world's saline lakes, *Nat. Geosci.*, 10(11), 816–821,  
717 <https://doi.org/10.1038/ngeo3052>, 2017.

718 Xiao, M., and Cui, Y.: Source of evaporation for the seasonal precipitation in the Pearl River Delta, China,  
719 *Water. Resour. Res.*, 57(8), e2020WR028564, <https://doi.org/10.1029/2020WR028564>, 2021.

720 Xie, F., Lu, P., Leppäranta, M., Cheng, B., Li, Z. J., Zhang, Y. W., Zhang, H., and Zhou, J. R.: Heat budget  
721 of lake ice during a complete seasonal cycle in lake Hanzhang, northeast China, *J. Hydrol.*, 620(18),  
722 129461, <https://doi.org/10.1016/j.jhydrol.2023.129461>, 2023.

723 Yang, K., Hou, J. Z., Wang, J. B., Lei, Y. B., Zhu, L. P., Chen, Y. Y., Wang, M. D., and He, X. G.: A new  
724 finding on the prevalence of rapid water warming during lake ice melting on the Tibetan Plateau, *Sci.*  
725 *Bull.*, 66(23), 2358–2361, <https://doi.org/10.1016/j.scib.2021.07.022>, 2021.

726 Yang, K., Wu, H., Qin, J., Lin, C. G., Tang, W. J., and Chen, Y. Y.: Recent climate changes over the  
727 Tibetan Plateau and their impacts on energy and water cycle: A review, *Global. Planet. Change.*, 112, 79–  
728 91, <https://doi.org/10.1016/j.gloplacha.2013.12.001>, 2014.

729 Zhang, Q., and Liu, H.: Seasonal changes in physical processes controlling evaporation over inland water,  
730 *J. Geophys. Res–Atmos.*, 119(16), 9779–979, <https://doi.org/10.1002/2014JD021797>, 2014.

731 Zhu, L., Yang, K., Wang, J. B., Lei, Y. B., Chen, Y. Y., Zhu, L. P., Ding, B. H., and Qin, J.: Quantifying  
732 evaporation and its decadal change for Lake Nam Co, central Tibetan Plateau, *J. Geophys. Res–Atmos.*,  
733 121(13), 7578–7591, <https://doi.org/10.1002/2015JD024523>, 2016.

---

734 **Figure Legends**

735 **Figure 1. Location of Qinghai Lake (below) and the measurement site of the Chinese Torpedo**  
736 **Qinghai Lake test base (upper).** The insets in the upper picture are photos of the four-way radiometer  
737 and infrared thermometer (left), meteorological variable measurements (middle), and eddy covariance  
738 sensors (right). The scale is just for the Qinghai Lake Basin.

739 **Figure 2. Diurnal characteristics of evaporation (E), latent heat flux (LE), sensible heat flux (H),**  
740 **heat storage change (G), and net radiation (Rn) of Qinghai Lake (QHL) during the ice-free and**  
741 **ice-covered periods (IFP and ICP) from 2014 to 2018.** The multiday average 30-min data during the  
742 IFP and ICP in each cycle year are shown here, and the colored shading indicates a 0.5 standard deviation.  
743 The gray area indicates nighttime. The labels 2014/2015, 2015/2016, 2016/2017, 2017/2018, and  
744 2018/2019 indicate the cycle year of the freeze-thaw cycles.

745 **Figure 3. Evaporation (E) rate (a, c, and e) and annual E sum (b, d, and f) of Qinghai Lake (QHL)**  
746 **during the cycle year (annual: AN), ice-free and ice-covered periods (IFP and ICP) in each cycle**  
747 **year from 2014 to 2018.** a and b show daily data, c and d show daytime data, and e and f show nighttime  
748 data. The whiskers in a, c, and e show the 1.5 interquartile range, while the letter associated with the  
749 whiskers indicates statistically significant differences via one-way ANOVA during the different freeze-  
750 thaw periods in each year from 2014 to 2018. The labels 2014/2015, 2015/2016, 2016/2017, 2017/2018,  
751 and 2018/2019 indicate the cycle year of freeze-thaw cycling.

752 **Figure 4. Sensitivity coefficient between the daytime and nighttime climatic factors and**  
753 **evaporation (E) rate of Qinghai Lake (QHL) during the ice-free and ice-covered periods (IFP and**  
754 **ICP).** \*, \*\*, and \*\*\* indicate statistical significance at the  $P < 0.1$ ,  $P < 0.05$ , and  $P < 0.01$  levels,  
755 respectively, via Student's t tests. Rn,  $\Delta e$ , WS, WD, Pres,  $T_a - T_s$ , Tl, and ICR indicate the net radiation,  
756 vapor pressure difference, wind speed, wind direction, Pres, difference between the air and lake surface  
757 temperatures, average temperature of the lake body from 0 to 300 cm, and ice coverage rate, respectively.

758 **Figure 5. Interannual variability in the simulated evaporation (E) rate (a-c) and annual E sum**  
759 **(d-f) of Qinghai Lake (QHL) in the cycle year (annual: AN), ice-free and ice-covered periods (IFP**  
760 **and ICP) from 2003 to 2017.** The blue shading indicates a 0.5 standard deviation, and the red shading

---

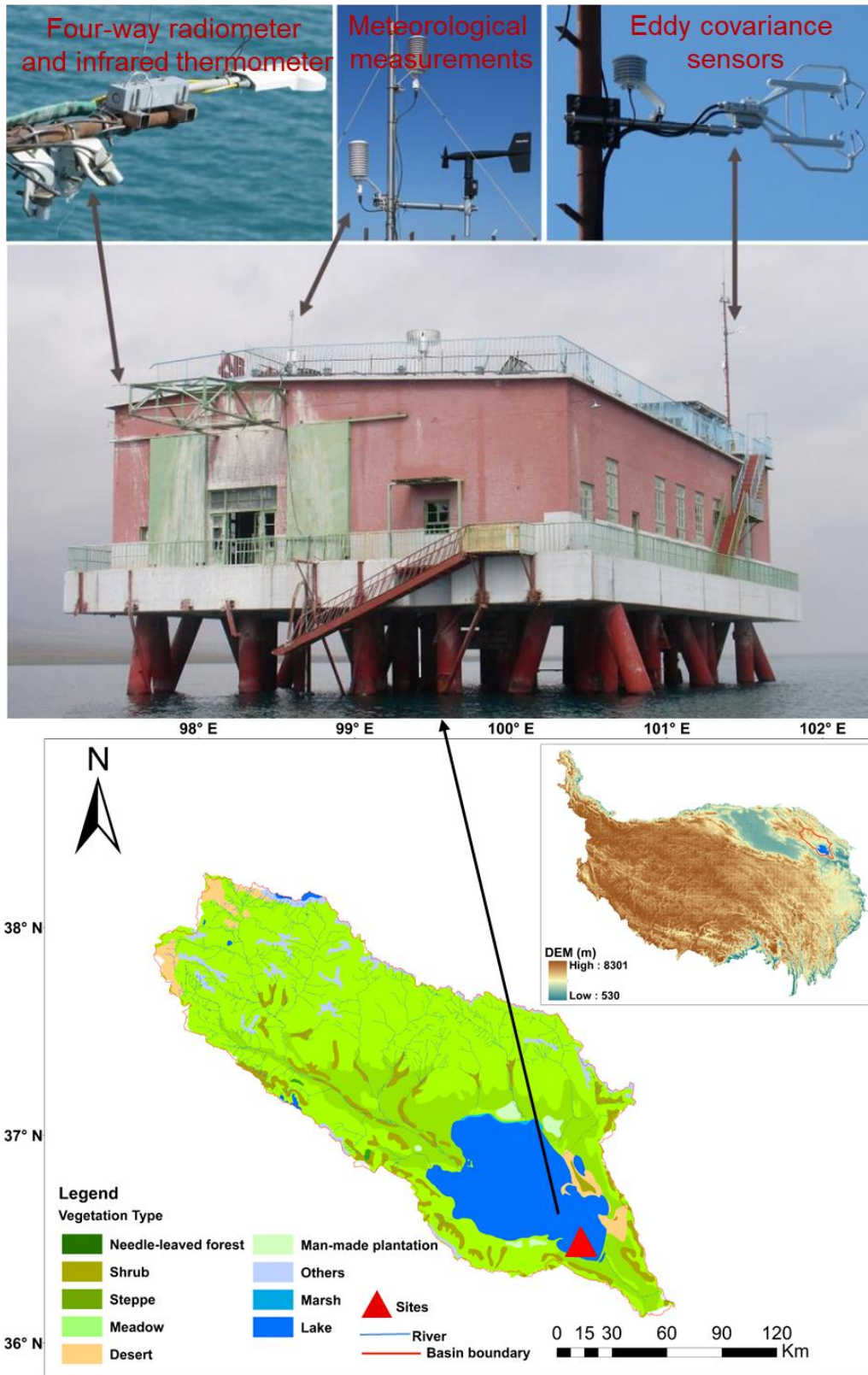
761 indicates the 95% confidence interval of the trend line.

762 **Figure 6. Evaporation (E) and heat storage change (G) in Qinghai Lake (QHL) during the ice-free**  
763 **and ice-covered periods (IFP and ICP).** WS, Pres,  $\Delta e$ ,  $T_a - T_s$ , Rn, and ICR are the wind speed, air  
764 pressure, vapor pressure difference, difference between  $T_a$  and  $T_s$ , net radiation, and ice coverage rate of  
765 the lake, respectively. The red plus sign indicates a positive effect of the variable on E.

766 **Figure 7. The multiyear average contribution of the changes in air temperature ( $T_a$ ), lake surface**  
767 **temperature ( $T_s$ ), downward shortwave radiation (Rs), and wind speed (WS) to the simulated**  
768 **evaporation (E) of Qinghai Lake (QHL) in the cycle year (annual: AN), ice-free and ice-covered**  
769 **periods (IFP and ICP) from 2003 to 2017.** a shows the multiyear average change in the E rate caused  
770 by  $T_a$ ,  $T_s$ , Rs, and WS; b shows the multiyear average change in the annual E sum caused by  $T_a$ ,  $T_s$ , Rs,  
771 and WS; and c shows the multiyear average change percentage of E caused by  $T_a$ ,  $T_s$ , Rs, and WS. The  
772 whiskers indicate a 0.5 standard deviation.

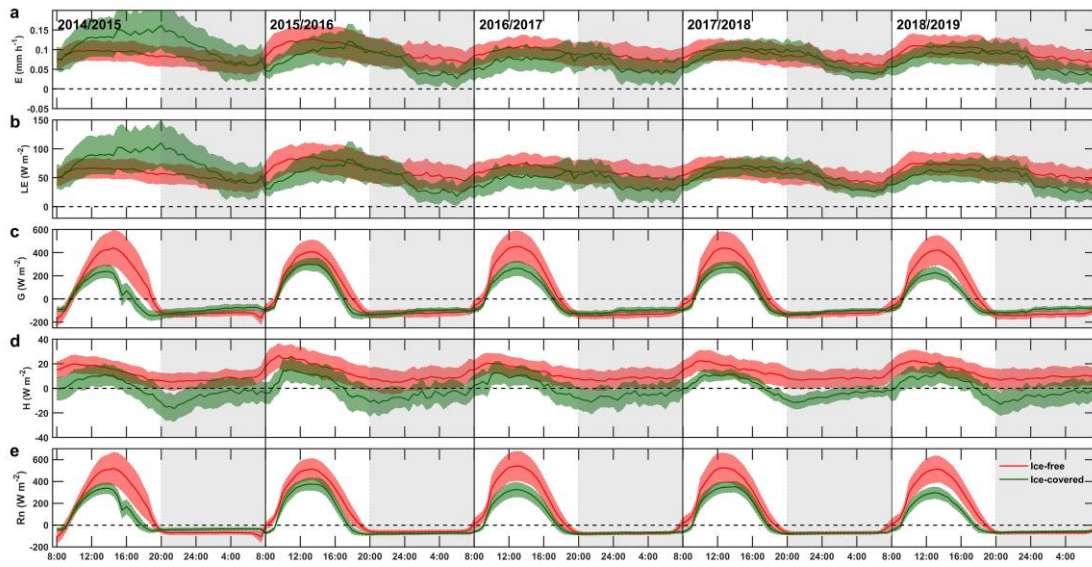
773 **Figures**

774 **Figure 1.**



775

776 **Figure 2.**

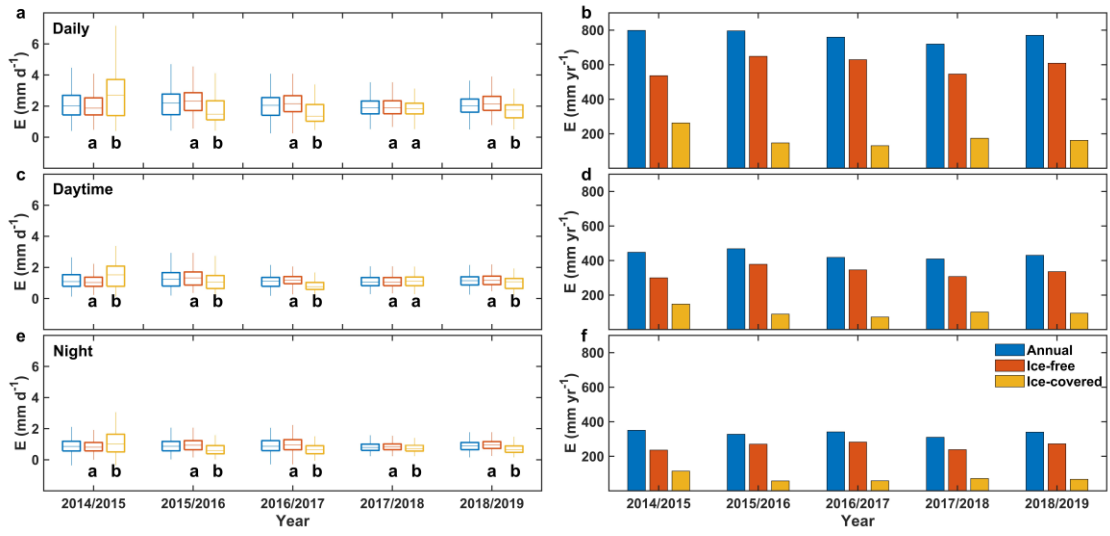


777

778

779

780 **Figure 3.**

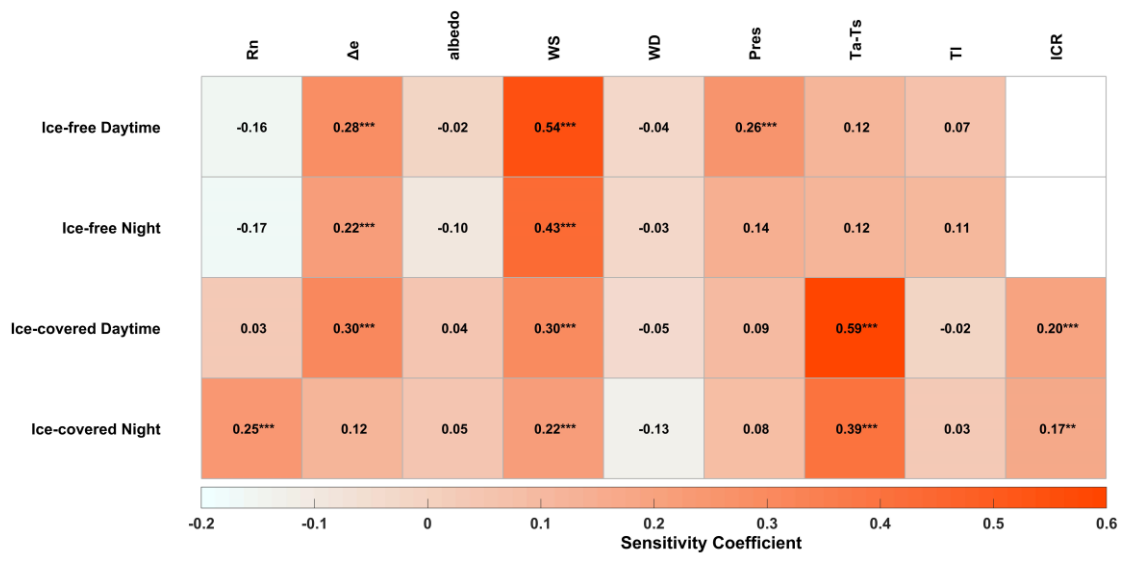


781

782



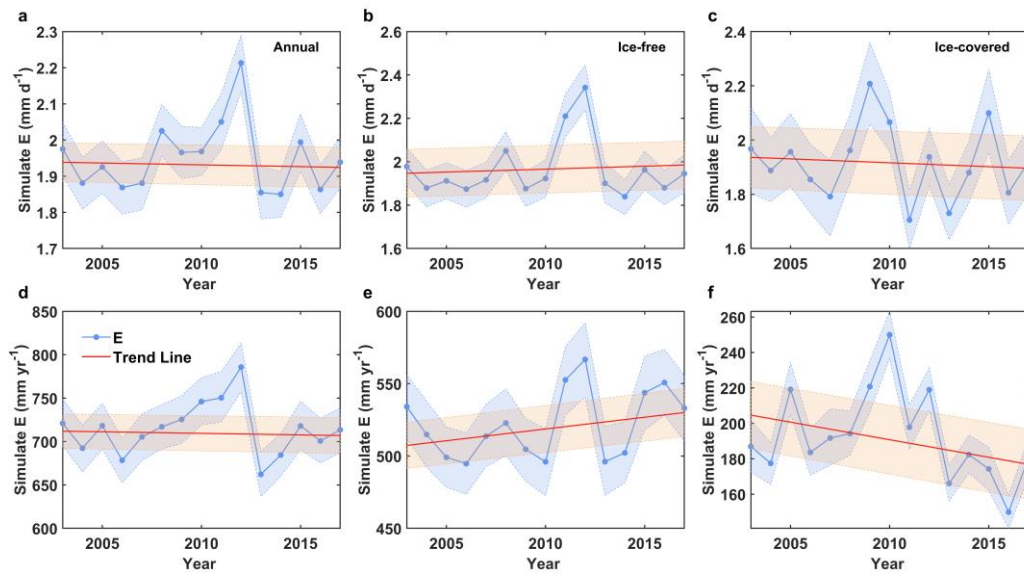
783 **Figure 4.**



784

785

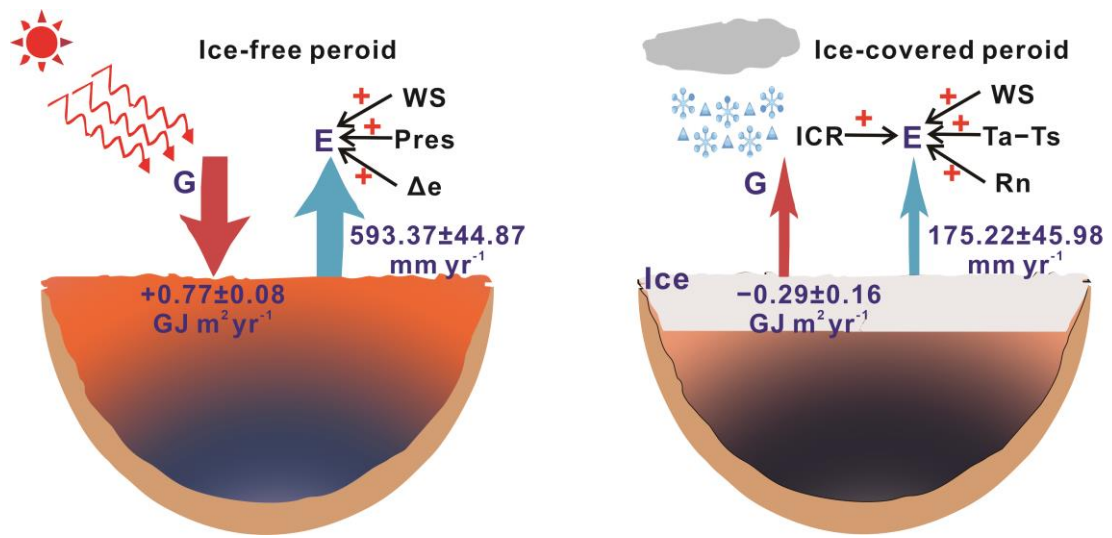
786 **Figure 5.**



787

788

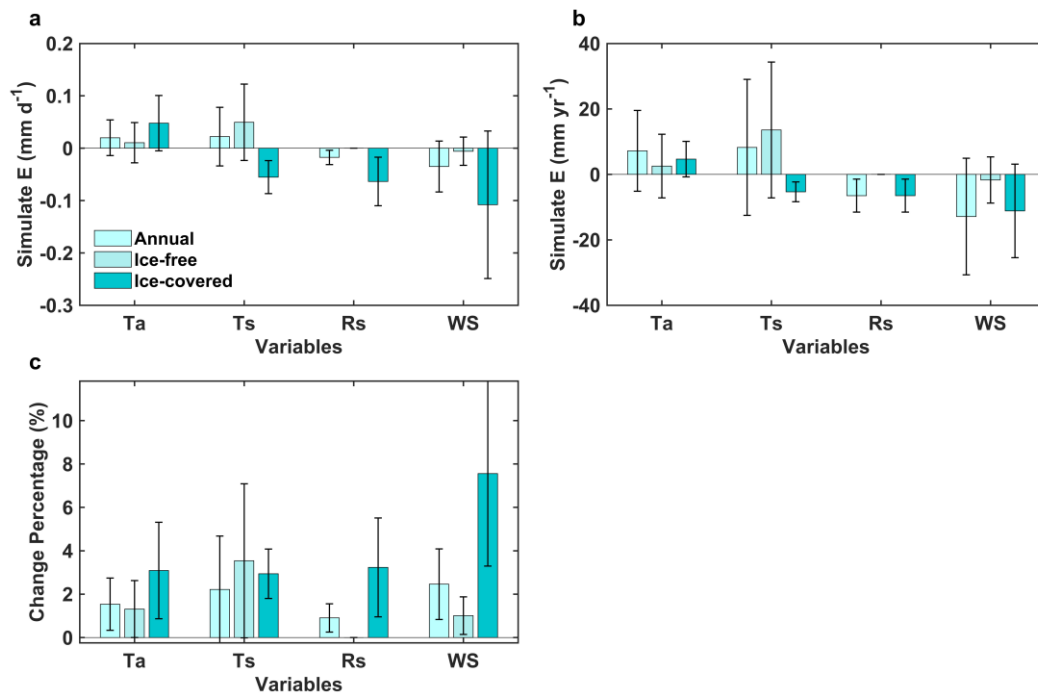
789 **Figure 6.**



790

791

792 **Figure 7.**



793

794